J Mater Sci (2022) 57:18323–18342

Chemical routes to materials

Reusable Schiff base probe implanted mesoporous materials for the optical detection and extraction of trace copper(II)

Aswanidevi Kongasseri[1], Prabhakaran Deivasigamani[1,*], and Akhila Maheswari Mohan[1,*]

[1] *Department of Chemistry, School of Advanced Sciences, Vellore Institute of Technology (VIT), Vellore, Tamil Nadu 632014, India*

Received: 11 July 2022
Accepted: 19 September 2022
Published online: 8 October 2022

ABSTRACT

The present study focuses on the detection and concentration of Cu^{2+} from contaminated waters using a D-π-A Schiff base probe, i.e., 2,3-bis(((E)-4-(diethylamino)-2-hydroxybenzylidene)amino) malononitrile (DAHAM) infused onto an ordered network of silica/polymer monolithic frameworks (S/PMFs). The tunable structural features, uniform surface morphology, voluminous porosity and excellent stability features of the monolithic frameworks (MFs) are well suited to function as probe anchoring templates for the sensing of ultra-trace concentrations of Cu^{2+}. The dense homogeneous arrangement of DAHAM molecules onto the surface sites of MFs transforms into a portable solid-state colorimetric sensor material for Cu^{2+} detection. The study reports a comparative evaluation of chromoionophore-modified silica/polymer MFs for the colorimetric sensing of Cu^{2+}. The DAHAM acts as chelating probe centers forming an octahedrally coordinated complex with Cu^{2+}, where the binding events are staged within the MF platforms. The $-NEt_2$ and $-C\equiv N$ groups of the DAHAM probe ensure conjugated electron transfer through D-π-A characteristics, thus providing concentration proportionate visual color transitions upon Cu^{2+} chelation. The solid-state sensors are selective for Cu^{2+}, with exceptional stability even under adverse conditions. The sensors reflect a recovery value of $\geq$ 99.2% in on-site real sample monitoring and are reusable for eight cycles, with excellent data reproducibility and reliability.

Handling Editor: Christopher Blanford.

Address correspondence to E-mail: prabhakaran.d@vit.ac.in; akhila.maheswari@vit.ac.in

https://doi.org/10.1007/s10853-022-07765-w

GRAPHICAL ABSTRACT

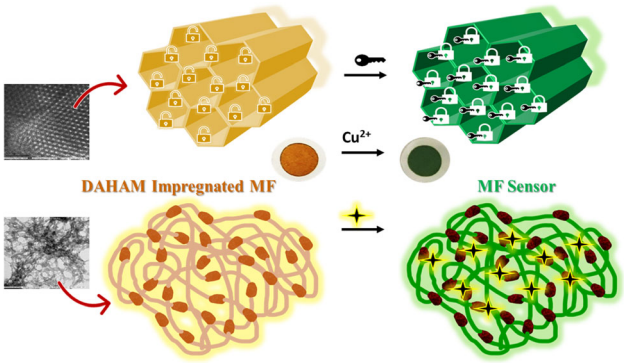

Introduction

Environmental serenity has been challenged drastically in the current era, causing the natural elements to be infected with various contaminants [1]. The meteoric growth of civilization pinned through the industrial revolution induced the possibility of heavy metal poisoning of quality-assured water sources. As water is an essential constituent for the sustenance of life, anything that pollutes water and enters the food chain/web is extremely deadly and demands immediate action [2]. The bioaccumulation and cross-reactive properties of heavy metal ions (HMIs) inside the body arouse critical interest in the scientific community to eliminate their false positives [3, 4]. In this line, Cu^{2+} is one of the essential HMI for human biological processes. It possesses well-defined roles in oxidative stress-related enzymatic processes such as hemoglobin production, carbohydrate metabolism and catecholamine biosynthesis [5, 6]. Besides, copper is an essential nutrient for photosynthesis and human metabolism. In humans, copper deficiency can lead to several issues, including abnormal bone growth, impaired coordination, loss of sensation and muscle fatigue [7]. However, as per WHO and US EPA statements, copper ions can be harmful if present beyond their permissible range of 1.0–1.3 mg/L. Hence, if present beyond the allowable limit, the reactive oxygen species produced by copper ions can stimulate various toxicological issues, thereby damaging biological macromolecular substances [8, 9]. Thus, it contemplates the necessity for checking the presence of copper ions in the soil and water environment.

Over the years, several techniques have been available to quantify copper ions from various environmental samples, using sophisticated analytical methods such as atomic absorption, microwave plasma atomic emission, inductively coupled plasma emission and surface plasmon resonance. Despite the excellent sensitivity associated with the analytical instruments, the high-cost factors, tedious sample preparation/pretreatment protocols, spectral/chemical inference and the necessity for skilled technicians make them less attractive for on-site routine analysis and real-time monitoring processes [10–14]. Recently, instrument non-dependent colorimetric sensors are becoming a promising detection tool for the common populace. In this aspect, liquid-based and nanoparticle-based sensors have evolved over the years by providing well-established color transitions with a reasonable degree of sensitivity. However, these approaches are non-reusable despite being user-friendly. Besides, they create additional secondary waste by using organic solvents, and the high dispersity index of NPs makes the sensing task tedious [15]. Even though the literature reports are enriched with excellent receptors with some common binding sites such as azo, amides, imines, triazoles, amidourea, thiourea, phenolics, indoles, azo-imines and pyrroles, the posh detection principle, delayed response, etc. restrict their applicational window [16–19]. Recently, Mahnashi et al. designed an imidazole-derived colorimetric and fluorometric

chemical sensor for Cu^{2+} with a color change to blue (λ_{max} 610 nm) with a detection limit (LOD) of 1.01 nM. Even though the chemical sensor shows good sensitivity and selectivity with the formation of a 2:1 complex, the reusability properties of such liquid-based sensors are still doubted [20]. Some researchers extend the liquid-phase mediated assay of Cu^{2+} to test strip analysis for a much more viable on-site analytical usage. For example, Liu et al. developed a test paper device based on a squarine-based probe with a color change from blue to faint yellow [21]. A similar kind of azo-based [22], Schiff base-assisted [23] and amide-based [24] liquid chemosensors are also available, which create secondary pollutants (organic solvents) besides inducing compatibility issues while dealing with natural aqueous systems. Besides, the test strip method was crude and lacked relatable authenticity and reliability. In addition, there are congruent methodologies, such as electroanalytical devices [25], photoacoustic nanoprobe designs [26], fluorogenic probe-assisted devices [27] and carbon dots [28], for the determination of inorganic analytes. However, the issues with these approaches are limited to extensive instrumental support, in a few cases, resulting in secondary pollutants with no guarantee for reusability [29]. The limitations mentioned above narrow the path for sensor designing, which can be resolved through synergizing material science with ligand chelation chemistry, thus paving the way for sensor materials with better sensing efficiency. Besides, the non-toxicity, accessible modification opportunities, reusability and brief analysis behavior are the critical features for the evolution of such hybrid material systems.

Keeping this in mind, the concept of solid-state colorimetric sensors can be a better alternative as they can be reusable without creating any secondary damage to environmental sources by attaching a chromoionophore to a solid porous template. The approach can lead to opto-chemosensors based on the metal–ligand complex's optical properties. In this aspect, monolith materials are excellent solid-state platforms due to their organized structural patterns of mesopore channels, allowing easy analyte diffusion to the chromoionophoric sites. The superior surface area associated with these monolithic materials can enhance the detection sensitivity and eliminate the possibility of secondary pollutants in the form of excess organic solvents. These porous organic/inorganic materials can serve as an efficient host template in anchoring the probes through various non-covalent interactions, thus facilitating the reusability features of the resulting solid-state sensor materials for several cycles without losing their sensing integrity. Few articles circumvent monoliths as solid-state colorimetric frameworks for Cu^{2+} detection [30]. Awual et al. developed a quinoline derivative incorporating porous silica monolith for Cu^{2+} sensing and removal [31]. Similarly, Sompalli et al. designed three organic receptors, which are implanted onto porous polymer monoliths for the visual sensing of Cu^{2+}, which substantiates the easy diffusive nature of polymer pores [32]. However, no reports elucidate the comparative study of mesoporous inorganic (silica-based) composite motifs and bimodal macro-/mesoporous organic (carbon-based polymer) monolithic frameworks incorporated with organic receptor molecules.

Therefore, in this work, we envisioned an alternative approach by developing an innovative and inexpensive solid-state naked eye responsive colorimetric sensor based on silica/polymer monolith impregnated with a structurally designed chromoionophoric probe for the sensing and preconcentration of Cu^{2+} ions in aqueous samples circumventing the expensive instrumental aid. The proposed solid-state sensors are the first to deploy bis-imino-based tetradentate probe scaffolds anchored onto the silica/polymer monolithic templates for Cu^{2+} sensing. The chemoresponsive sensor proffers chromatic color change from pale yellow to bright green on the incremental addition of Cu^{2+} under optimized analysis conditions. The excellent sensitivity and the exclusive ion selectivity of the proposed naked eye sensor motifs mark a better solution for the current need for an eco-/user-friendly, low-cost and reliable approach to pollution monitoring.

Experimental

Chemicals and instrumentation

All the chemicals, solvents and reagents are AR-grade and used without further purification. For the preparation of silica-based inorganic monolithic framework, tetraethyl orthosilicate (TEOS; silica precursor), Pluronic P123 ($(EO_{20}PO_{70}EO_{20})$; structure-dictating agent), triisopropylbenzene (TiPB; Porogen) are

obtained from Sigma-Aldrich. For the synthesis of polymer-based organic monolithic frameworks, acrylic acid (monomer), butyl methacrylate (monomer), ethylene glycol dimethacrylate (cross-linker) and azobisisobutyronitrile (radical initiator) are procured from TCI chemicals. Chemicals such as 4-(diethylamino) salicylaldehyde and diaminomaleonitrile are procured from Sigma-Aldrich for synthesizing the chromoionophoric probe (DAHAM). The pH adjustments are made using buffers of 0.2 M $ClCH_2COOH$-HCl (pH 1–3), CH_3COONa-CH_3COOH (pH 4–6), MOPS-NaOH (pH 7–9) and CHES-NaOH (pH 10–11). Ultra-pure water (18.2 MΩ.cm) is used for the analytical procedures. The metal ion solutions used for the analytical testing are of AAS grade (1000 ppm) bought from Sigma–Aldrich.

The phase transition measurements for the prepared MFs and sensor materials are analyzed using a powder X-ray diffractometer (p-XRD; Bruker, D8 Advance). Identifying functional groups associated with the MFs and probe molecules is conducted using a Fourier transform infrared spectrophotometer (FT-IR; Shimadzu, Spectrum). The structural and surface morphological features of the MFs are imaged using a field emission scanning electron microscope (ZESS EVO18) and a high-resolution transmission electron microscope (FEI-Tecnai, G^2 20 Twin). The surface area and pore dimensional measurements are conducted using the BET/BJH method (Quantachrome, Autosorb iQ TRx). The sensor's elemental presence and chemical (oxidation) states are resolved using an X-ray photoelectron spectrometer (XPS, PHI 5000, VersaProb-II). The structural characterization of the probe is performed using an NMR spectrophotometer (Bruker, Ascend 400 MHz) and CHNS elemental analyzer (Elementar Vario, Micro Select EL). The analytical optimizations are conducted using a UV–visible diffuse reflectance spectrophotometer (UV–Vis DRS, Jasco, V730). The authentication of actual sample compositions is confirmed using an inductively coupled plasma mass spectrometer (ICP-MS; Agilent 7900).

Synthesis of chromatic probe (DAHAM)

The chromatic ligand (**DAHAM**) is synthesized via a simple, one-pot condensation reaction of 4-(diethylamino)salicylaldehyde **(A)** and diaminomaleonitrile **(B)**. A 1.0 mM of **B** in 10 mL ethanol is added dropwise to an ethanolic solution of 2.1 mM of **A**, and the reaction is allowed to continue for 24 h at room temperature. The precipitated product (DAHAM) is purified by successive washing with hexane. The complexation of Cu^{2+} with DAHAM involves ligand-to-metal charge transfer transition (LMCT), where the electron flow occurs from both imine (–C = N) and hydroxyl (–OH) groups of the probe molecules to the vacant metal *d* orbitals of Cu^{2+}. The schematic representation of the probe synthesis and its Cu^{2+} complexation process is depicted in **Scheme 1**.

The structural confirmation and purity of DAHAM are decided using various spectroscopic techniques. **DAHAM** (Yield: 94%). **^{1}H NMR (400 MHz, DMSO)**, δ: 11.26 (s, 2H), 9.44–9.52 (d, 2H), 7.32–7.46 (d, 2H), 6.31–6.54 (d, 2H), 6.02–6.20 (d, 2H), 3.31–3.6 (m, 8H), 1.01–1.31 (m, 12H). **^{13}C NMR (400 MHz, DMSO)**, δ: 164.52, 154.21, 133.43, 126.47, 115.34, 109.19, 104.65, 99.83, 48.51, 12.96. **FT-IR:** C≡N (2204 cm^{-1}), C = N (1652 cm^{-1}), C-N (1232 cm^{-1}), O–H (3414 cm^{-1}). **Elemental Analysis,** %C: 69.24 (68.10), %H: 6.42 (6.59), %N: 18.49 (18.33), %O: 6.54 (6.98). The theoretical elemental composition of the probe molecules is denoted in the parenthesis.

Synthesis of silica monolithic frameworks (SMFs)

SMF is prepared using the microemulsion-based sol–gel method by direct templating process, using P123 as the surface/structural dictating soft template. For SMF synthesis, 1.5 g of P123 and 0.8 mL of TiPB are homogenized, followed by the dropwise addition of 4.5 mL of 1 M HNO_3 and 1 mL of H_2O to form a gel-like residue. A 4 mL of TEOS is added to the reaction mixture under continuous stirring, thus initiating rapid exothermic hydrolysis and condensation

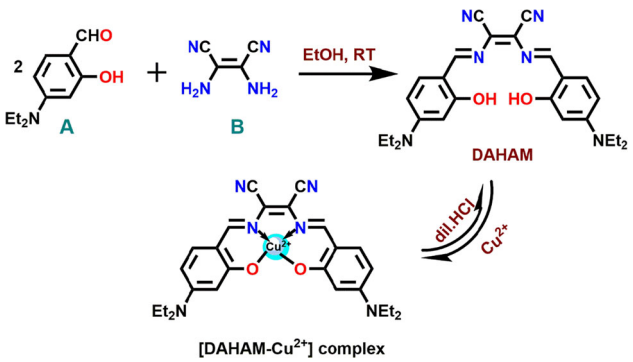

Scheme 1 Synthesis representation of DAHAM probe molecules and their complexation with Cu^{2+}.

[33, 34]. The obtained sol–gel is subjected to an aging process at 40 °C for 24 h, thus promoting the formation of a highly ordered inorganic monolithic network around P123, followed by removing the by-product (ethanol), thus leading to a macro-level arrangement of mesopores. The temperature-controlled calcination offers the desired mesoporous silica monolithic framework (SMF). During calcination, the destruction or shrinkage of SMF is prevented through a controlled temperature ramping of 2 °C/min, which is held at 550 °C for 8 h to remove the organic/inorganic impurities. The resulting crack-free SMF is structurally characterized using microscopic and spectroscopic techniques.

Synthesis of polymer monolithic frameworks (PMFs)

PMF is synthesized via a simple thermal-assisted free radical bulk polymerization technique. The monomeric mixture of 0.05 mM of acrylic acid and butyl methacrylate is dissolved in a 15 mL DMF and DMSO (1:1) porogenic mixture. A 1 mM of EGDMA (cross-linker) is added dropwise to the monomer–porogen solution and allowed to homogenize for 0.5 h. The monomer–cross-linker stoichiometry is kept at 1:10, where the two monomers are at a 1:1 ratio. Further, the mixture is added with 0.3 mM of AIBN (initiator) under constant stirring. The pre-polymerization mixture is purged with N_2 gas to remove dissolved oxygen that could hinder the polymerization process. The mixture is allowed to stir at room temperature for 2 h, followed by thermal treatment at 85 °C for 24 h. The high temperature induces the polymerization process with bimodal macro-/mesopores [35, 36], thus forming PMFs.

Sensor material fabrication

The sensor material is fabricated by disseminating the DAHAM probe onto SMF/PMFs through a direct impregnation process of non-covalent interactions. For this process, a known concentration (0.01–0.3 mmol) of DAHAM molecules in ethanol is equilibrated with 1.0 g of SMF/PMFs for 2 h. Further, the solvent is removed using a rota-evaporator to seal an effective heterogeneous multi-phase impregnation of probe molecules in a uniform pattern across the monolithic framework. The resulting materials are water-washed to remove any loosely adsorbed/loaded DAHAM probe molecules. The washed product is vacuum dried at 40 °C for 6 h to yield the sensor materials for ion sensing applications. The quantity of ligand loaded onto the monolithic framework is calculated using the following equation,

$$Q_t = \frac{(C_o - C_t)V}{G} \cdot (mmol/g)$$

where Q_t is the quantity of ligand loaded, C_o denotes the initial ligand concentration, C_t denotes the threshold ligand concentration, V depicts the total volume of the solution and G defines the mass of monolithic material employed.

Sample pretreatment procedure and sample analysis

The water samples (river water, lake water and industrial wastewater) are filtered using 0.22 µm membrane filter paper to remove the dispersed particles and are stored at low temperatures (10 °C). The water sample pH is adjusted before analysis, and the samples are spiked with appropriate concentrations of Cu^{2+} and proceeded for sensor studies under optimized analytical conditions. The obtained results are correlated with ICP-MS analysis for data reliability and accuracy.

For the naked eye sensing and spectral analysis, 3–4 mg of optimized probe-loaded MFs (sensor materials) is dispersed onto a series of 20 mL aqueous solution consisting of 5 mL of proper buffer, along with proportionate concentrations of Cu^{2+} (0–500 ppb) that are equilibration in an orbital shaker for 5 min at 120 rpm. The blank (without Cu^{2+}) sensor is used to comparatively find and quantify the presence of Cu^{2+} in various analyte samples. The metal ion solution equilibrated sensor materials are filtered through membrane filter paper (25 mm dia., 0.45 µm pore) and analyzed using the UV–Vis-DRS instrument. The analytical properties that could influence the solid-state sensing process are perfected by studying the role of pH, kinetics, temperature, probe content, sensor quantity, matrix tolerance, linear response range, detection and quantification limit. A pentaplicate measurement protocol has been adopted to confirm the reliability and repeatability of the analytical data.

Results and discussions

Analysis of surface and structural features of MFs and sensor materials

The surface morphological features of the synthesized MFs are studied using FE-SEM and HR-TEM analysis [37, 38]. Figure 1a, b shows deep intertwined cave-like patterns for the polymer monolith, thus allowing easy trapping of probe scaffold within the bimodal macro-/mesopores. The pattern favors anisotropic ligand trapping, easing interconnected diffusion across the ordered layers of monolith framework. These properties assess the syllogism associated with sensitive detection and coordination chemistry. The dense macro-porous voids present on the surface of polymer monolith are uniform, revealing the possibility of ordered flow/diffusion of the analyte, thus enhancing the kinetic efficiency. Figure 1c, d shows the FE-SEM images of a silica monolith as a fibril-like porous pattern of a continuous network that ensures easy probe molecules' encapsulation. FE-SEM images certify the possibility of maximum probe binding ability of the PMF and SMF materials, thus promoting the multi-channel diffusion of target analytes, thus ensuring a visual sensing approach with faster response kinetics and sensitivity. The HR-TEM images Fig. 1e, f of PMF show an orderly, arranged, regularly interconnected ringlike bimodal network of macro-/mesopores. This feature enhances the surface and bulk diffusion of the target analyte to the probe molecules that are uniformly coordinated/adsorbed on the monolithic framework. For SMF, the HR-TEM images Fig. 1g, h reveals a highly ordered and interconnected honeycomb-like continuous arrangement of hexagonal mesoporous channels that allow easy diffusion of analytes to the uniformly hosted probe molecules.

The monoliths' probe adsorption efficiency and ion diffusion properties are analyzed through the BET isotherm pattern (Fig. 2a–d), enumerating the surface area and porosity features [39, 40]. For SMF, the N_2 adsorption–desorption isotherm studies carried out at 77 K reveal an H_1 hysteresis loop with a type IV isotherm pattern with a surface area of 332.76 m^2/g. However, with incorporating the DAHAM probe, albeit a decrease in the surface area to 240.61 m^2/g. In the case of PMF, a surface area of 270.10 m^2/g is obtained, followed by a decline to 241.68 m^2/g upon probe anchoring. The observed decline might be due to the reduction in the surface-exposed pores of the MFs upon the systematic incorporation of the probe molecules. The pore properties assessed through BJH calculations yield an effective average pore diameter of 6.05 and 4.57 nm for SMF and PMF, respectively, with pore volumes of 0.608 and 0.418 cm^3/g. Likewise, the probe immobilized MFs show a marginal decline in the pore diameter value (5.21 and 3.85 nm) with a slight decrease in the pore volume (0.402 and 0.252 cm^3/g) for PMF and SMF, respectively.

The SAED pattern (Fig. 3a, b) reveals the absence of bright spots to confirm the amorphous nature of the SMF/PMF materials, which are in corroboration with the p-XRD data, as depicted in Fig. 3(c, d). The p-XRD pattern for MFs reveals broad humped typed peaks, centered at (2θ), 21.9° and 27.5° for SMF and PMF, respectively, confirming their amorphous character. It is seen that upon probe anchoring, the diffraction peak shifts to (2θ) 22.9° and 28.6° for SMF and PMF, respectively. The slight redshift in the diffraction peak can be attributed to the occupancy of the probe moieties on the MF network, which

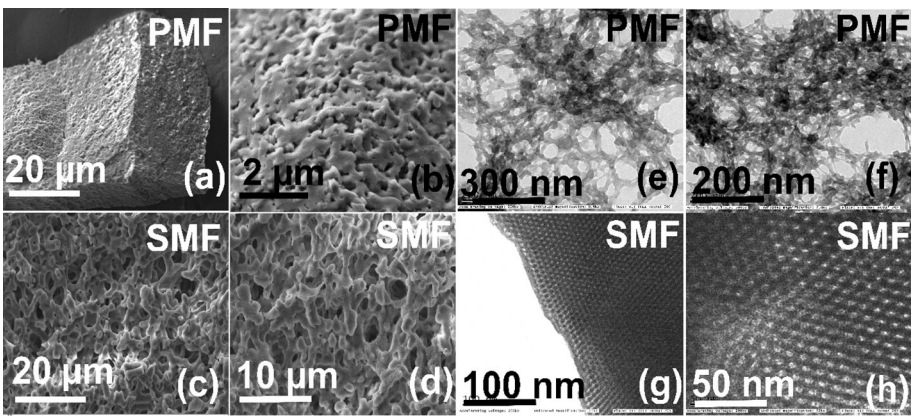

Figure 1 FE-SEM images of varying resolutions of **a**–**b** polymer monolithic framework (PMF) and **c**–**d** silica monolithic framework (SMF). HR-TEM images of varying resolutions of **e**–**f** PMF and **g**–**h** SMF materials.

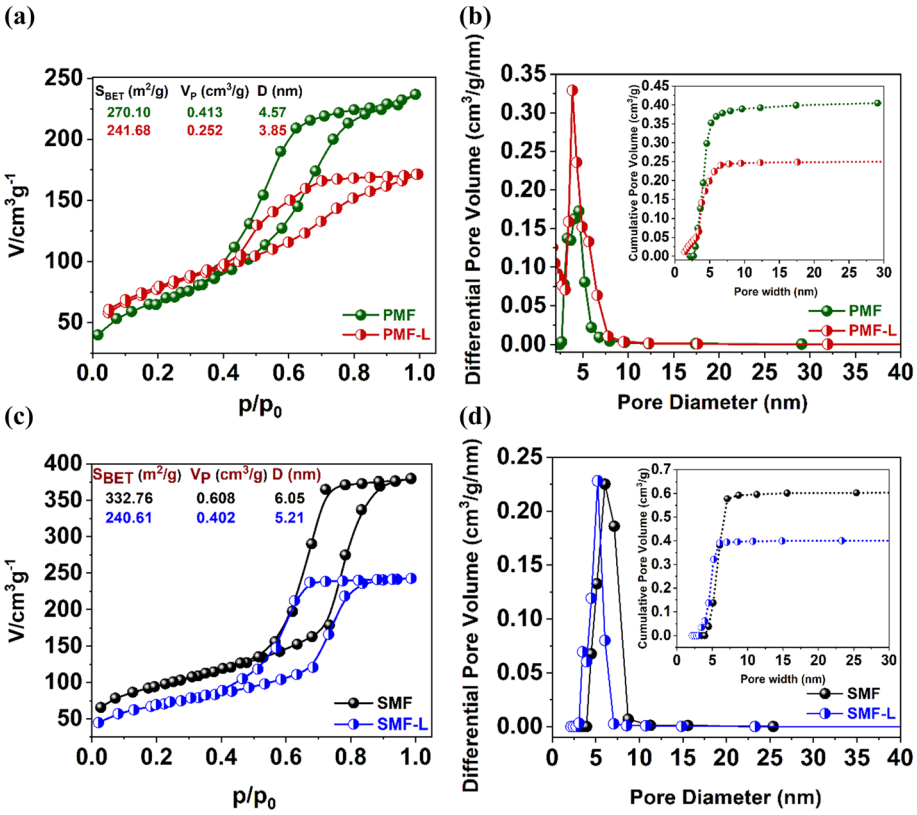

Figure 2 **a** and **c** N_2 adsorption–desorption isotherm and **b** and **d** BJH pore size distribution of bare and ligand-loaded polymer and silica monolithic frameworks, respectively.

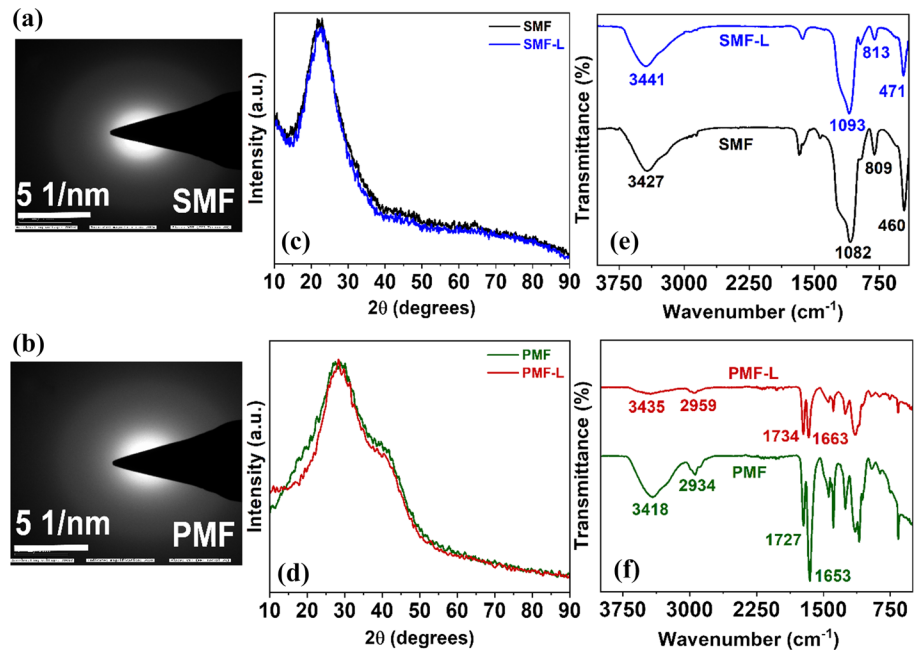

Figure 3 SAED pattern of **a** silica monolith and **b** polymer monolith materials. Wide angle *p*-XRD spectra of **c** bare and ligand-loaded silica monolith and **d** bare and ligand-loaded polymer monolith. FT-IR spectra of **e** bare and ligand-loaded silica monolith and **f** bare and ligand-loaded polymer monolith.

deviates from the diffraction path of the incident X-ray beam. The redshift in 2θ values in MFs after probe loading can be attributed to the shortening of the average bond distance of the MF due to its electrostatic interaction with the probe molecules.

FT-IR spectral analysis for SMF, PMF and their corresponding probe-loaded MFs denoted as SMF-L and PMF-L has been conducted to learn their functional groups associated with the material. For SMF, Fig. 3e shows symmetric and asymmetric stretching

vibration peaks at 809 and 1082 cm^{-1} for the Si–O–Si backbone, which experiences a marginal redshift and a decrease in peak intensity upon ligand anchoring (SMF-L). A similar shift in peak position and intensity is seen for the bending vibration of the Si–O–Si framework (460 cm^{-1}) and the stretching vibration of Si–OH (3427 cm^{-1}) units of the surface silanol groups (SMF). For PMF (Fig. 3f), the C=O stretching vibrations corresponding to the monomer/cross-linker are seen at 1653 cm^{-1}, while the O–C=O ester stretching vibration for the EGDMA backbone is seen at 1727 cm^{-1}. The $–CH_2$ asymmetric stretching vibration is reflected at 2934 cm^{-1}, where the various–CH_2 bending vibrations are seen below 1500 cm^{-1}. The peak at 3418 cm^{-1} corresponds to the O–H stretching vibrations of the adsorbed water molecules in PMF. The physical changes in IR peak profiling due to ligand loading did not influence the appearance of any other vibrational peaks due to the low content of ligand loading to the MFs. However, the heteroatoms in the DAHAM interact with the functional group moieties of the MFs, thus ensuring effective interaction and confined orientation with the porous framework that favors selective interaction with Cu^{2+} ions. Hence, the high surface area and voluminous porosity features of MFs define the high-performance aspect of capturing and sensing Cu^{2+} ions by the MF modifier (probe molecules). The MFs facilitate easy ion diffusion through the mesopore channels for complexation with probe molecules dispersed through intermolecular interactions. The sterically hindered frozen conformations of the probe molecules within the MFs centers facilitate exclusive selectivity during the ion sensing process, thus restraining the interference from other chemically reactive species.

The confirmation of the elemental presence and their oxidation states in the Cu^{2+} complexed SMF-/PMF-L materials are checked through XPS analysis (Fig. 4a–l) [41]. The XPS survey spectra for the Cu^{2+} complexed SMF-L and PMF-L sensor materials are depicted in Fig. 4a. From the binding energy profile and the intensity of the photoelectron peaks, it can be concluded that the Cu^{2+} complexed SMF-L material confirms the elemental presence of Si2*p*, O1*s*, C1*s*, N1*s* and Cu2*p* orbital states, with a relative composition of 21.2, 67.7, 9.6, 0.1 and 1.5%, respectively. Similarly, the Cu^{2+} complexed PMF-L material confirms the existence of the C1*s*, O1*s*, N1*s* and Cu2*p* orbital states, with a relative composition of 71.4, 26.8, 0.1 and 1.6%, respectively. The high-resolution XPS data show the chemical and electronic state of the elements, which supply further insight into the mode of binding and sensing processes. Here, the PMF sensor shows intense peaks for C1*s* of the C–C skeleton at 284.66 eV and low-intensity peaks at 285.95 eV (C–O) and 288.72 eV (O–C=O) of the EGDMA backbone (Fig. 4b). The O1*s* deconvolution spectra (Fig. 4c) show the presence of two peaks at 533.91 and 532.32 eV, corresponding to the C–O–C and O–C=O groups, respectively. The deconvoluted XPS data (Fig. 4d) for the Cu^{2+} complexed probe anchored MFs reveal two binding energy peaks at 936.06 and 956.17 eV corresponding to the Cu2$p_{3/2}$ and Cu2$p_{1/2}$ orbital states, respectively. The changes in the electronic environment of the imide nitrogen atoms (N1*s* energy state) of DAHAM molecules have been critically evaluated before and after the complexation of Cu^{2+} ions, as shown in Fig. 4e–f. The N1*s* XPS data of Cu^{2+} uncomplexed PMF-L material reveals a single peak at 399.34 eV, corresponding to the –C = N– unit of the DAHAM molecules. However, for the DAHAM-Cu^{2+} complex, an additional satellite peak is observed at 404.44 eV for the PMF sensor. Besides, the N1*s* binding energy peak of the –C = N– unit shows a slight red shift to 399.94 eV, thus confirming the Cu^{2+} complexation through –C = N– coordination. An intense deconvoluted peak at 103.16 eV confirms the presence of the Si–O–Si network within the SMF-L material, which corresponds to the Si2$p_{3/2}$ orbital state, along with a smaller peak at 104.32 eV, which in turn corresponds to Si2$p_{1/2}$ of the terminal Si–OH groups (Fig. 4g). The O1*s* orbital state of the SMF sensor has been deconvoluted to two peaks positioned at 532.88 eV and 534.01 eV, corresponding to the oxygen atoms of Si–O–Si and Si–OH groups (Fig. 4h). The chelation of Cu^{2+} ions in the SMF sensor has been inferred through the presence of Cu2*p* orbital state peaks, i.e., Cu2$p_{3/2}$ and Cu2$p_{1/2}$ with binding energy at 934.96 and 955.34 eV, respectively (Fig. 4i). The C1*s* peak of the DAHAM probe anchored onto the SMF template exhibits an intense binding energy peak at 285.58 eV (Fig. 4j). In the case of SMF-L material, the N1*s* orbital state shows an intense peak at 398.61 eV (Fig. 4k) before Cu^{2+} complexation. However, after complexation with Cu^{2+} ions, a new satellite peak appears at 407.47 eV, along with a red shift in N1*s* binding energy to 400.33 eV, which corresponds to the C=N unit of DAHAM molecules (Fig. 4l). Besides, the

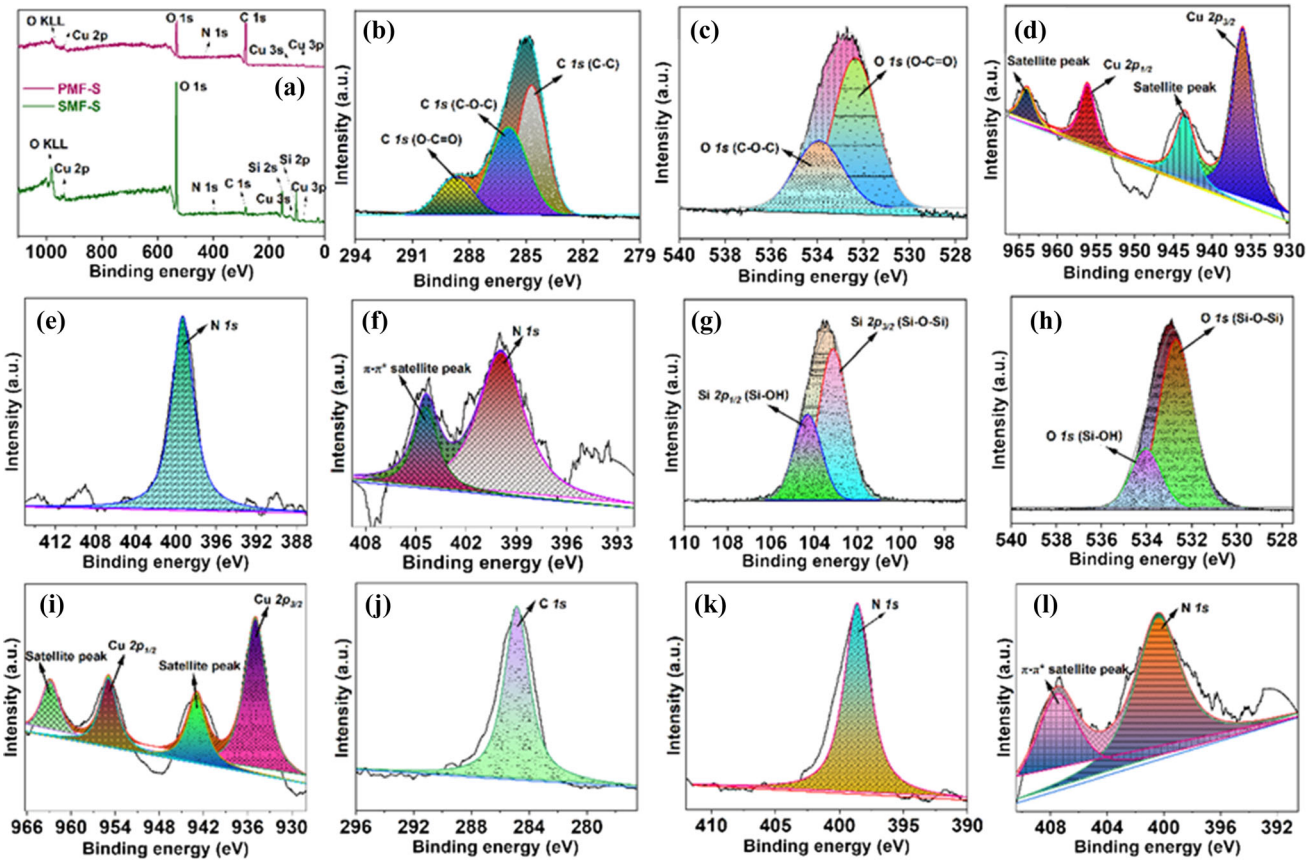

Figure 4 **a** Wide range XPS spectra of silica and polymer monolithic sensors. High-resolution XPS spectra of **b** C*1s*, **c** O*1s*, **d** Cu2*p*, **e** N*1s* (before treatment with Cu^{2+}) and **f** N*1s* (after treatment with Cu^{2+}) orbital states of polymer monolithic sensor. High-resolution XPS spectra of **g** Si2*p*, **h** O*1s*, **i** Cu2*p*, **j** C*1s*, **k** N*1s* (before treatment with Cu^{2+}) and **l** N*1s* (after treatment with Cu^{2+}) orbital states of silica monolithic sensor.

uniform distribution of elements across the MFs is inferred through elemental mapping (Fig. 5a–g, and the elemental composition and the purity state of MFs are further confirmed using EDAX (Fig. 5h, i).

Optimization of analytical parameters for solid-state ion sensing

The sample pH is vital for sensitivity and selectivity factors during ion sensing. It can change the surface charge interactions of MFs and probe molecules, paving the way for the dominant existence of various target analyte species interacting differently with the sensor materials [42]. In an aqueous media, copper can exist in multiple forms such as Cu^{2+}, $Cu(OH)_2$, $CuCO_3$, $[Cu(OH)_4]^{2-}$ and $[Cu(CO_3)_2]^{2-}$. The presence of these species in coherence can be expected in the sample solution. However, the predominant existence of a particular species may vary according to the solution pH. As real samples can have a wide range of pH

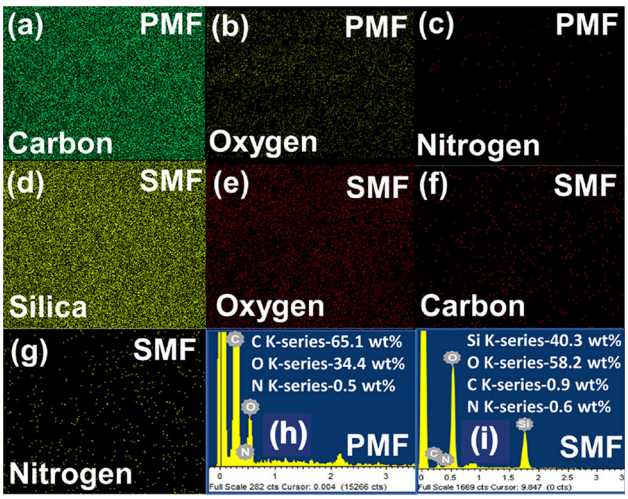

Figure 5 Elemental mapping of **a** carbon, **b** oxygen, **c** nitrogen, **d** silica, **e** oxygen, **f** carbon and **g** nitrogen of PMF and SMF sensor materials, respectively. EDAX spectra of **h** PMF and **i** SMF sensor materials.

depending on environmental factors, perfecting sample pH is crucial for consistent and reliable interpretations. In this line, optimization studies are performed using varying pH (3.0–9.0) of Cu^{2+} solutions equilibrated with sensor materials, as discussed in Sect. 2.6. Figure 6a shows a steep increase in the signal/colorimetric response for the sensor material in Cu^{2+} sensing, as the solution pH varied from 3.0 to 6.0, with a maximum response at pH 7.0. Beyond pH 7.0, a steady decline in the colorimetric response is seen, thus confirming the best ion sensing response at neutral pH, where copper predominately exists in its Cu^{2+} form. At neutral pH, the lone pair of electrons associated with the imine nitrogen, along with the hydroxyl oxygen atoms of DAHAM molecules, chelate with Cu^{2+} ions, thus resulting in ligand-to-metal charge transfer electronic transitions. Under acidic conditions (< 7.0), the H^+ ions will effectively protonate the chelating centers of DAHAM, thereby reducing the chances of DAHAM-Cu^{2+} complexation. Conversely, in alkaline pH, the Cu^{2+} forms stable hydroxy complexes of $Cu(OH)_2$, $Cu(OH)_3^-$ and $Cu(OH)_4^{2-}$, thus disabling the possibility of complex formation.

The solution temperature is a crucial parameter in defining ion sensing kinetics and efficiency, which has been assessed by equilibrating the sensor materials with a known concentration of Cu^{2+} (100 ppb) as a function of increasing temperature (15 to 45 °C), as depicted in Fig. 6b [43, 44]. At T ≥ 30 °C, the proposed sensor assemblies show faster ion response kinetics. However, at T ≤ 250 °C, a prolonged equilibration is needed for the sensor materials to produce the largest signal response for Cu^{2+} ions. The observed data prove the working efficiency of the proposed sensor materials across a wide range of solution temperatures with a shorter analysis time, thus substantiating its real-time on-site monitoring capabilities. The faster signal response with increasing temperature is rationalized to the rapid diffusion phenomena of the analytes through the solution medium due to the transference of thermal energy into kinetic energy. However, the solvated analytes are saturated with thermal gain beyond a temperature range, thus revealing a flat response profile. Further, the uniform alignment of meso-/macropores in the MFs manages fast ion sensing. The hexagonal

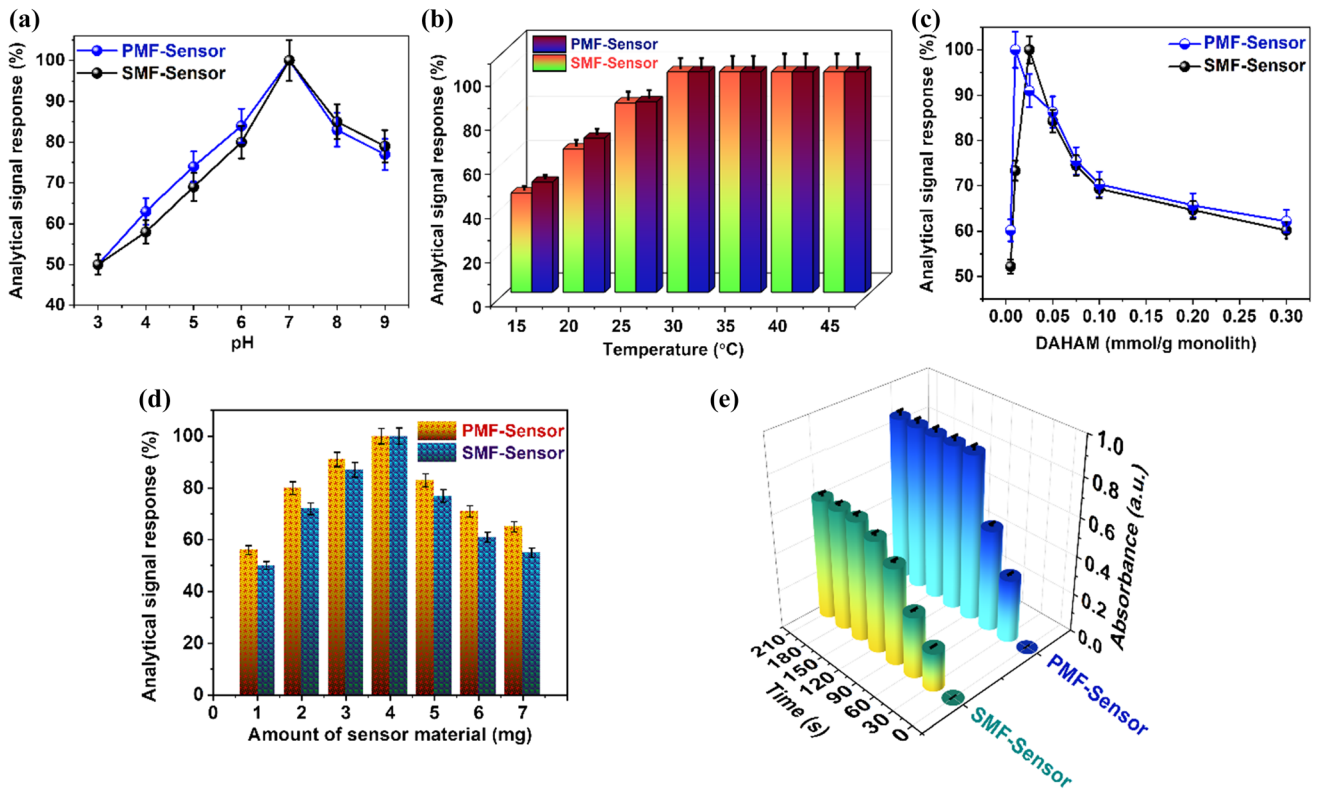

Figure 6 Effect of **a** pH of the sensor media, **b** temperature, **c** probe (DAHAM) concentration, **d** quantity of sensor material and **e** time on Cu^{2+} detection.

pores of the SMF network and the ringlike spherical pores of the PMF framework ensure fast kinetics through easy diffusion of the analyte and accessibility toward the active ligand sites through the aqueous medium. Particularly, the macropores throughout the PMF network proffers fast kinetics of sensing (compared to SMF sensor) through better interaction of the metal ions with the chelating sites of the anchored DAHAM molecules. In this line, the amount of the probe embedded in the monolith matrix also plays a key role, which is assessed by loading a series of probe concentrations (0.005–0.3 mM of DAHAM) onto the MFs to assess their sensing efficiency. Figure 6c reveals a largest signal response with 0.010 and 0.025 mM probe concentrations for PMF-L and SMF-L sensor materials. The better signal response in the initial stages of probe concentrations is attributed to the adequate availability of probe chelating sites for the ultra-trace sensing of Cu^{2+}, thus leading to color transitions. The observations are authenticated with the high surface area of the MF motifs through which uniform distribution of the ligand moieties is made possible. However, the colorimetric/signal response shows a retarding/declining effect beyond the above-indicated critical probe concentrations due to overpowering the original color of the non-complexed DAHAM molecules that suppresses the Cu^{2+}-DAHAM color transitions.

The individual sensor quantity needed for efficient ion sensing is studied using 1.0–7.0 mg of SMF-/PMF-L sensor materials. Under optimized analytical conditions, the assessment benefits the sensitive naked eye colorimetric detection of target ions. Figure 6d shows that a lower sensor material dosage (1.0–3.0 mg) yields a lower signal response with minimum spectral/colorimetric intensity due to insufficient probe chelating sites for metal ion chelation. However, at 4.0 mg, a maximum signal and colorimetric profile response is seen for SMF and PMF sensors. The threshold sensor dosage (4.0 mg) certifies the availability of adequate probe molecules per dosage for the efficient sensing and quantitative assessment of the target analyte. The high surface area and porosity features of the MFs facilitate sufficient probe loading that warranties efficient optical response for the target analyte while using a minimal quantity (4.0 mg) of the sensor material. However, beyond 4.0 mg, a decline in the response profile is due to the excess probe molecules, which can be avoided by tuning the sensor dosage as per the analysis requirement. However, for bulk preconcentration procedures, a higher probe concentration or sensor dosage allows the voluminous recovery/encapsulation of Cu^{2+} using the proposed sensor materials, which can also function as ion concentrators.

Under optimized analytical conditions, the variation in sensor performance as a function of time is assessed in the period up to 210 s, as shown in Fig. 6e [45]. A steady increase in the sensing performance is noticed from the plot with increasing equilibration time, reaching a maximum within 90 and 150 s for PMF-L and SMF-L, respectively. Interestingly, the sensor shows excellent visual color transitions within seconds, which is challenging to obtain in solid-state ion sensing. The best rationale for this observation is the ordered structural design of the proposed MFs of uniformly arranged meso-/macropores, which eases the analyte diffusion through the aqueous media to the probe sites present in the inner layer of the MFs. The minimal time observed for sensing Cu^{2+} on the PMF sensor can be attributed to the faster diffusion of the analyte through the uniform macroporous network.

Concentration proportionate calibration plot and ion selectivity studies

The selective probe chelation with Cu^{2+} and its visual color transitions can be tuned by creating well-defined specific cavities for the target, with restricted receptor flexibility and specific hardness/softness associated with the coordinating atoms [46]. The synthesized ligand DAHAM is a π-conjugated tetradentate [O^N^N^O] chelating bis-Schiff base ligand, which has two covalent and two coordinate covalent sites situated in a planar array. Under optimized analytical conditions, the variation in the absorption spectra (UV–Vis-DRS) for the proposed sensor materials as a function of Cu^{2+} concentrations (0–500 ppb) has been investigated. Figure 7a, b shows that the metal-free sensor shows a peak maximum (λmax) at 435 nm, corresponding to the π–π* electronic transitions associated with the DAHAM molecules, revealing a deep orange color for the blank sensor. However, with the incremental addition of Cu^{2+} concentration, the sensor shows a series of color transitions from deep orange to brown and deep green, which is elucidative from the visual color change images (Fig. 7c, d). The UV–Vis-DRS data

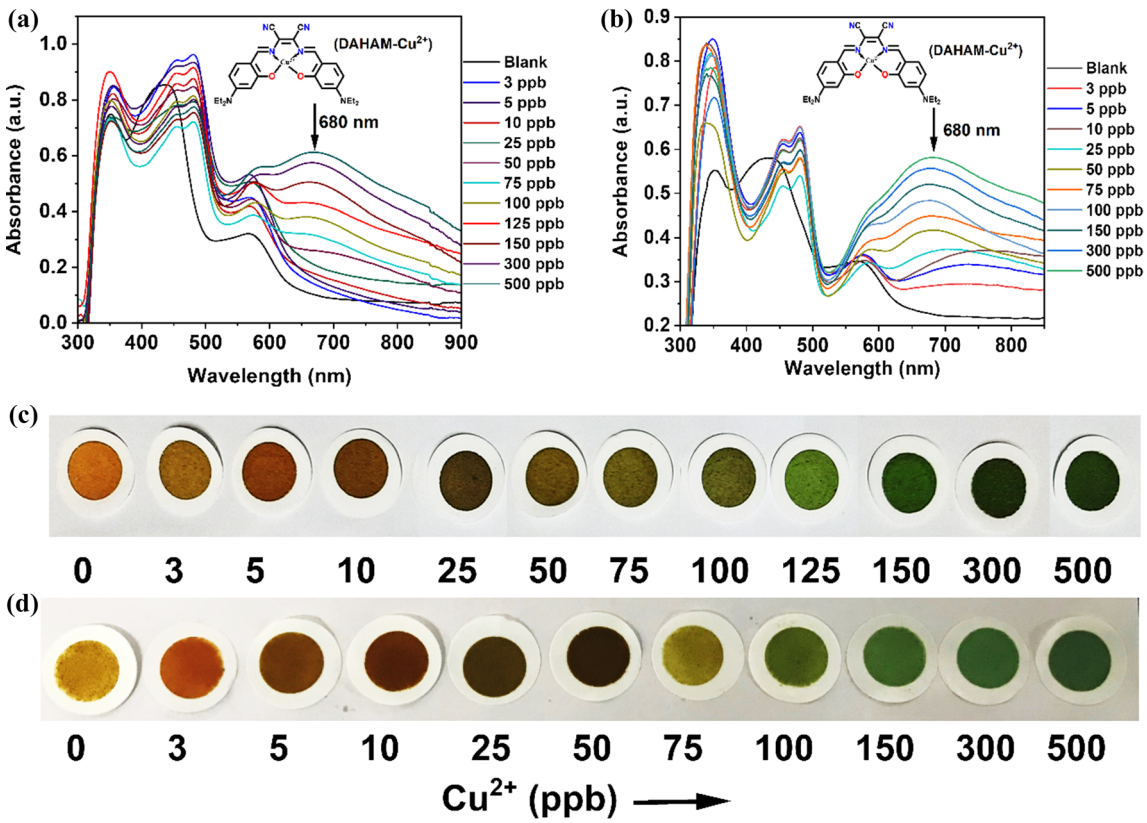

Figure 7 Cu^{2+} concentration proportionate UV–Vis-DRS response on **a** polymer monolithic sensor, **b** silica monolithic sensor. **c** and **d** Naked eye color change as a function of Cu^{2+} concentration for polymer and silica monolithic sensors, respectively.

shows a hyperchromic shift for peaks at 455 nm and 480 nm with the appearance of a new peak at 680 nm that corresponds to the green-colored Cu^{2+}-DAHAM complex. The color transitions are associated with the ligand–metal charge transfer transition process from the probe's electron-rich imine nitrogen and hydroxy oxygen atoms to the vacant *d* orbital of the Cu^{2+} state. The appealing and drastic color change (n–π* electronic transitions) upon metal complexation is ascribed to the presence of electron-donating $–NEt_2$ and –CN functional groups in the para position of the DAHAM molecule, making it electron-rich for Cu^{2+}complexation. The stoichiometric binding between the receptor probe (DAHAM) and Cu^{2+} ions is studied by Job's continuous variation method *(Electronic Supporting Information)*. The results reveal the formation of a stable 1:1 complex where the Cu^{2+} ion is encapsulated in the probe coordination sites, forming a strong chelate effect, a typical scenario seen in supramolecular and macromolecular systems (such as porphyrin). The stoichiometric binding ratio is substantiated by ^{1}H NMR titration *(Electronic Supporting Information)*, which shows the participation of the two hydroxyls and imine moiety of the DAHAM probe. The Benesi–Hildebrand method shows a strong binding affinity of Cu^{2+} with ligand DAHAM with a binding constant of $2.59 \times 10^3\ M^{-1}$, as discussed in *Electronic Supporting Information*.

For the quantitative analysis of the ultra-trace concentrations of Cu^{2+} ions, the linear response range is studied by a calibration plot for the sensor material as a function of Cu^{2+} concentrations under optimized analysis conditions (Fig. 8a, b). The plot indicates a linear response profile for the sensor in the Cu^{2+} concentration range of 3–150 ppb, with a corresponding slope value (m) of 0.00268 and 0.00199 for PMF and SMF sensors, respectively, with r^2 of 0.999 and 0.998, respectively. Using the limit of detection (LOD) and quantification (LOQ) equations (LOD = 3 σ/m; LOQ = 10 σ/m), the LOD and LOQ value for the PMF sensor is calculated as 0.11 and 0.37 ppb, respectively. In the case of the SMF sensor, the LOD and LOQ values are estimated as 0.75 and 2.51 ppb, respectively. The lower LOD value associated with the PMF sensor is attributed to the structural and surface features of the translucent polymer

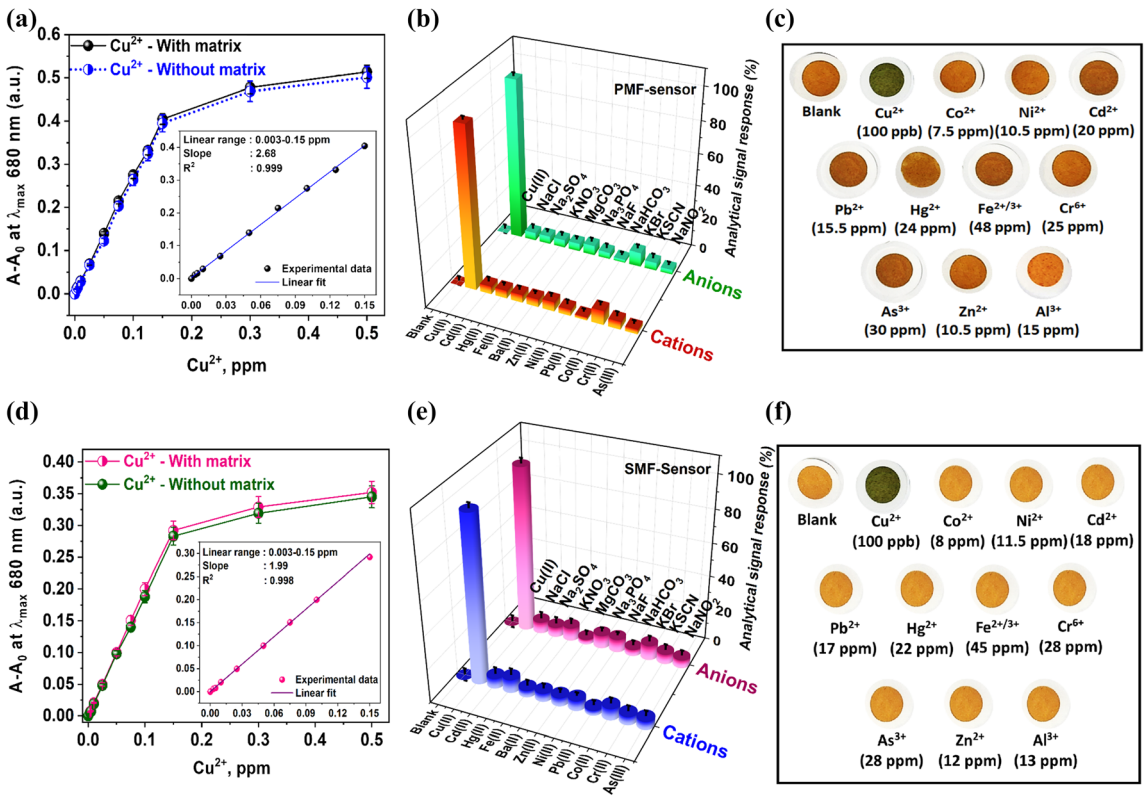

Figure 8 Calibration plot and linear fit (inset), the effect of interfering matrix ions (cations and anions) on sensor's performance and images pertaining to the color change in response to the addition of other metal ions for **a**–**c** polymer and **d**–**f** silica monolithic sensors, respectively.

monolith framework, which is an advantageous factor in assisting the ion sensing process. The obtained analytical data using the proposed method is compared with the literature-reported sensory motifs of various methods, as tabulated in Table 1. The comparison data reflect the superior analytical features of the proposed sensing method for the quantitative sensing and recovery of ultra-trace Cu^{2+} ions.

Even though there are numerous reasons for choosing porous architectures as solid templates for the sensing process, the primary reason is the extraordinary selectivity shown by these sensory platforms, which might otherwise not be possible in liquid-state sensory systems. The classical problem associated with selectivity is that the more sensitive a sensory system, the less robust it can be beyond a certain point. The selective probe response for Cu^{2+} ions in other cations and anions commonly met in real sample matrices has been evaluated with the proposed PMF (Fig. 8b, c) and SMF (Fig. 8e, f) sensors. The results reveal that the proposed sensor is a solution for linking the opposite demands where the selectivity is achieved over a wide concentration range without compromising the sensitivity of the detection process. The sensitivity is not altered in the presence of even higher concentrations of chlorides, nitrates and sulfates which reveals that any salts of Cu^{2+} can be potentially sensed using the proposed solid-state monolithic sensors. It is important to note that the tetradentate chelating DAHAM probe exhibits poor ion selectivity in the liquid-state medium. In a liquid medium (with bare ligand), the selectivity of Cu^{2+} detection is lost due to significant interference from Co^{2+}, Hg^{2+} and Fe^{3+} ions, thereby making the DAHAM nontarget-specific. However, when anchored onto the structurally engineered solid template of MFs, the encapsulated probe molecules within the porous architectures restrict the free rotation, minimizing the wide approachability of various metal ions to the coordination/chelating sites in a specific geometrical/spatial orientation. As a result of the frozen probe conformation within the mesopore network, the presence of multifold concentration of ions like Fe^{3+} (up to 48 ppm) did not exhibit any

Table 1 Comparison table portraying the analytical features of the proposed monolithic framework solid-state naked eye Cu^{2+} sensors with reference to the literature reports of other colorimetric methods/sensors

S. No	Method	Materials/probes used	Linear response range	Limit of detection	Ref
1	Peroxidase-like activity of Prussian blue nanocubes for colorimetric sensing of Cu^{2+}	Prussian blue nanocubes and tetramethyl benzidine	0.006–0.009 mM	0.0181 mM	[47]
2	Liquid-based colorimetric detection of Cu^{2+} using a Schiff base ligand	4-((2-hydroxynaphthalen-1-yl)methylene)amino)-4'-((-(1-hydroxynaphthalen-2-yl)methylene)amino)-[1,1'-biphenyl]-3,3'-diol	–	2.72 µM	[48]
3	Polyethyleneimine-Protected Silver Nanoclusters for Cu^{2+} detection	Hyperbranched polyethyleneimine-protected silver nanoclusters	10–7.7 µM	10 nM	[49]
4	ZnO@ZnS core–shell nanoparticles-based Cu^{2+} sensing	Disposable paper coated with ZnO@ZnS core–shell nanoparticles	15–1500 µM	15 µM	[50]
5	Colorimetric sensing of Cu^{2+} ions based on "CLICK-17" DNAzyme-catalyzed azide modified gold nanoparticles and alkyne capped dsDNA cycloaddition	(a) Method A (azide-AuNPs/alkyne-linker DNA/SA) (b) Method B (azide-AuNPs/alkyne-linker DNA/CLICK-17) (c) Method C (azide-AuNPs/alkyne-linker DNA/CLICK-17/SA)	(a) 15–100 mM (b) 0.20–1.25 mM (c) 0.05–0.5 mM	(a) 6.6 mM (b) 102 nM (c) 26.8 nM	[51]
6	Mesoporous conjugate material for selective optical Cu^{2+}ions monitoring	Mesoporous silica conjugated with N,N-disalicylidene-4,5-dimethyl-phenylenedene (DDPD)	31.47–1573.6 nM	5.03 nM	[52]
7	Sugar pyrazolin-5-one-based optical chemosensor for the detection of Cu^{2+}	Glyco conjugated pyrazoline-5-one derivative	0.1–1.0 µM	0.27 µM	[53]
8	D-π-A Schiff base conjugated mesoporous silica/polymer monoliths for Cu^{2+} detection	2,3-bis((-4-(diethylamino)-2-hydroxybenzylidene)amino)maleonitrile conjugated silica and polymer monolithic frameworks	**47.21–2360.3 nM**	**(a) 1.73 nM (PMF sensor)** **(b) 11.80 nM (SMF sensor)**	**Present work**

significant interference, which may be impossible with bare ligand-mediated sensing. The ion-selective color transitions upon Cu^{2+}-DAHAM complexation are unique as the solvatochromic probe molecules are frozen/trapped within the porous monolithic template structure.

The selectivity assay defines that the presence of other analytes over multitudes of concentration (100 times) greater than that of Cu^{2+} could not cause any severe interference or masking, thus indicating the exclusive selectivity of the proposed sensor motifs tabulated in Table 2. Based on the optimization results, the sensor performance has been confirmed with real water samples such as groundwater, lake water, river water, industrial wastewater and RO-treated water, along with daily consumption products such as tea leaves, honey and milk powder as depicted in Table 3. The analytical data from the sensor materials reveal a recovery range of 99.5–101.6%, with a relative standard deviation (RSD) of $\leq$ 2.2%. The results are rationalized by analyzing the sample using ICP-MS analysis to validate the proposed method. The results confirm that the synthesized SMF and PMF sensors were well suited for the colorimetric detection of Cu^{2+} in various aqueous samples.

Sensor reusability and stability studies

One of the attractive features of the solid-state sensors is the lack of conventional creation of secondary pollutants, with excellent reliability and reusability

Table 2 Tolerance limit of interfering foreign ions (electrolytes and metal ions) during the optical sensing of 100 ppb of Cu^{2+} ions

Common electrolytes			Common metal ions		
Electrolytes	Tolerance limit (ppm)		Metal ions	Tolerance limit (ppm)	
	PMF sensor	SMF sensor		PMF sensor	SMF sensor
NaCl	6900	6950	Pb^{2+}	15.5	17.0
Na_2SO_4	3050	3125	Zn^{2+}	10.5	12.0
$NaNO_2$	700	650	Co^{2+}	7.5	8.0
Na_2SO_3	900	925	Ni^{2+}	10.5	11.5
KSCN	450	460	Mn^{2+}	12.0	12.5
KNO_3	3300	3150	$Fe^{2+/3+}$	48.0	45.0
NaF	1000	1100	Cd^{2+}	20.0	18.0
$NaHCO_3$	1400	1500	Cr^{6+}	25.0	28.0
Na_3PO_4	6300	6500	Hg^{2+}	24.0	22.0
$MgCO_3$	1375	1400	$As^{3+/5+}$	30.0	28.0
KBr	1100	1200	Al^{3+}	15.0	13.0
CH_3COONa	4850	4600	Ca^{2+}	1000	1100
			Mg^{2+}	1100	1150

properties even after multiple analyses. In this context, the reusability performance of the sensor materials has been checked by equilibration with 100 ppb of standard Cu^{2+} solutions under optimized analytical conditions. The resulting color transitions are quantified by UV–Vis-DRS measurement. Subsequently, the Cu^{2+}-DAHAM complex is decomplexed by adding 1 mL of 0.1 M EDTA, resulting in a thermodynamically stable Cu^{2+}-EDTA complex. The metal-free sensor material is washed with deionized water and checked for the blank sensor material's initial color/spectral pattern using UV–Vis-DRS measurements. The process is repeated several times to check the sensor efficiency during the complexation and decomplexation process, as plotted in Fig. 9a. The plot shows the reliable and reproducible response efficiency for eight repeated cycles.

The DAHAM molecules have been physically immobilized onto the SMF and PMF template through non-covalent interactions (Vander Waal's force and hydrogen bonding). The ligand-loaded MF template was washed with deionized water to remove the unmodified or loosely attached ligand from the monolith surface. Due to the strong physical interaction of DAHAM with the MF surface, the ligand DAHAM did not leach out from the MF template for several cycles of repeated usage for ion sensing studies. However, beyond eight cycles, probe bleeding shows a slow and steady decline in sensor performance. Besides, the long-term stability of the sensor materials has been analyzed by storing them for over a year and periodically checked for their ion sensing and reusability efficiency (Fig. 9b). It is found that the SMF-based sensor materials are stable over an extended storage period compared to the PMF sensor materials, thus attenuating the durable lifetime of silica-based materials. The sensor materials were also assessed for their efficiency in various physiochemical conditions such as temperature and pH. From the observations, both the sensors exhibited stable behavior in the pH range of 2.0–10.0. However, beyond pH 2.0, the SMF sensor tends to be less stable, which might be due to the disintegration/hydrolysis of the Si–O-Si network. Also, the efficacy of SMF and PMF sensors remains unaltered in the temperature range of 10–60 °C. It is also noteworthy that the bare SMF material exhibits high thermal stability up to 200 °C. However, the PMF materials can only withstand temperatures up to 100 °C, restricting their utility to relatively low-temperature field applications. The reusability and durability features of the proposed sensors can reduce the cost factor associated with fabrication and analysis without compromising their ion-sensitivity/selectivity features, besides being eco-benign.

Conclusion

This article reports on two solid-state sensing protocols using inorganic/organic monolithic templates, a highly selective imine probe DAHAM and the

Table 3 Testing of actual samples from environmental and industrial sources for detecting and recovering trace concentrations of spiked Cu^{2+} ions

Sample Source	Matrix Ion Composition (ppm)	Cu^{2+} Spiked Amount (ppb)	Recovery (ppb) SMF-S	Recovery (ppb) PMF-S
Ground Water	**Cu^{2+}: 0.05 ppm**	0	$49.5^a \pm 1.1^b$	$49.8^a \pm 0.9^b$
	Zn^{2+}, Ni^{2+}: ≤ 0.09 ppm	10	$60.05^a \pm 1.3^b$	$60.3^a \pm 1.2^b$
	Mn^{2+}, $Fe^{2+/3+}$: ≤ 2.0 ppm	25	$75.29^a \pm 1.7^b$	$75.9^a \pm 1.5^b$
	Na^+, K^+, Mg^{2+}, Ca^{2+}: ≤ 430 ppm	50	$100.2^a \pm 1.9^b$	$100.8^a \pm 1.6^b$
	F^-, $NO_3{}^{2-}$, $PO_4{}^{3-}$: ≤ 135 ppm			
	Cl^-, HCO^{3-}, $CO_3{}^{2-}$: ≤ 295 ppm			
Lake Water	**Cu^{2+}: 0.075 ppm**	0	$75.1^a \pm 0.7^b$	$75.3^a \pm 0.9^b$
	Zn^{2+}, Ni^{2+}: ≤ 0.18 ppm	5	$80.6^a \pm 1.7^b$	$80.3^a \pm 1.1^b$
	Mn^{2+}, $Fe^{2+/3+}$: ≤ 1.5 ppm	15	$90.5^a \pm 1.5^b$	$90.2^a \pm 1.0^b$
	Na^+, K^+, Mg^{2+}, Ca^{2+}: ≤ 205 ppm	25	$100.3^a \pm 1.2^b$	$100.5^a \pm 1.5^b$
	F^-, Cl^-, $NO_3{}^{2-}$, $PO_4{}^{3-}$: ≤ 50 ppm	50	$125.2^a \pm 1.1^b$	$125.4^a \pm 1.8^b$
	$CO_3{}^{2-}$, HCO^{3-}: ≤ 160 ppm			
River Water	**Cu^{2+}: 0.08 ppm**	0	$80.1^a \pm 0.7^b$	$80.2^a \pm 0.9^b$
	Zn^{2+}, Ni^{2+}: ≤ 0.2 ppm	10	$90.4^a \pm 1.5^b$	$90.2^a \pm 1.0^b$
	Mn^{2+}, $Fe^{2+/3+}$: ≤ 1.3 ppm	30	$110.1^a \pm 0.7^b$	$110.6^a \pm 1.3^b$
	Na^+, K^+, Mg^{2+}, Ca^{2+}: ≤ 180 ppm	50	$130.9^a \pm 1.9^b$	$130.5^a \pm 1.2^b$
	F^-, Cl^-, $NO_3{}^{2-}$, $PO_4{}^{3-}$: ≤ 80 ppm			
	$CO_3{}^{2-}$, $HCO_3{}^-$: ≤ 145 ppm			
Industrial wastewater	**Cu^{2+}: 0.15 ppm**	0	$149.2^a \pm 0.9^b$	$147.8^a \pm 0.6^b$
	Zn^{2+}, Ni^{2+}: ≤ 0.5 ppm	5	$155.6^a \pm 0.8^b$	$155.8^a \pm 0.6^b$
	Mn^{2+}, $Fe^{2+/3+}$: ≤ 1.6 ppm	10	$159.7^a \pm 0.7^b$	$159.9^a \pm 0.5^b$
	Na^+, K^+, Mg^{2+}, Ca^{2+}: ≤ 190 ppm	20	$171.3^a \pm 1.5^b$	$170.3^a \pm 1.9^b$
	F^-, Cl^-, $NO_3{}^{2-}$, $PO_4{}^{3-}$: ≤ 70 ppm	30	$180.2^a \pm 2.0^b$	$179.7^a \pm 1.1^b$
	$CO_3{}^{2-}$, $HCO_3{}^-$: ≤ 150 ppm			
RO treated water	**Cu^{2+}: (n.d)***	0	0	0
	Mn^{2+}, $Fe^{2+/3+}$: ≤ 0.04 ppm	10	$9.8^a \pm 1.5^b$	$10.1^a \pm 1.2^b$
	Na^+, K^+, Mg^{2+}, Ca^{2+}: ≤ 50 ppm	20	$20.1^a \pm 1.1^b$	$20.6^a \pm 1.8^b$
		50	$49.2^a \pm 1.5^b$	$49.8^a \pm 0.8^b$

* n.d: not detected;

[a] Average of three measurements;

[b] Standard deviation

comparative advantages of excellent ion selectivity and simple naked eye colorimetric sensing. The proposed solid-state colorimetric approach can be widely adopted to examine and recover various analytes through physical and chemical modification of the MFs with chemosensitive probes of varying functionality. Here, we could reason the exclusive selectivity for Cu^{2+} using DAHAM probe molecules anchored onto the structurally designed porous MFs. It is also attenuated that choosing the proper materials (porous monolithic frameworks) allows restricted geometrical conformations to the probe molecules, which increases the potentiality for the selective detection of analytes. Moreover, electron-withdrawing π acceptors like NEt_2 and C≡N groups enhance the visual color transitions from deep orange to dark green, increasing concentrations of Cu^{2+}. The proposed portable and inexpensive reusable solid-state sensory systems will result in large-scale productions with broad utility for various environmental and industrial applications. In addition, the sensor material materials reflect faster response kinetics of a few seconds, a wide linear response range and excellent sensitivity in superior LOD and LOQ values. The proposed eco-friendly and cost-effective sensor materials' remarkable durability and

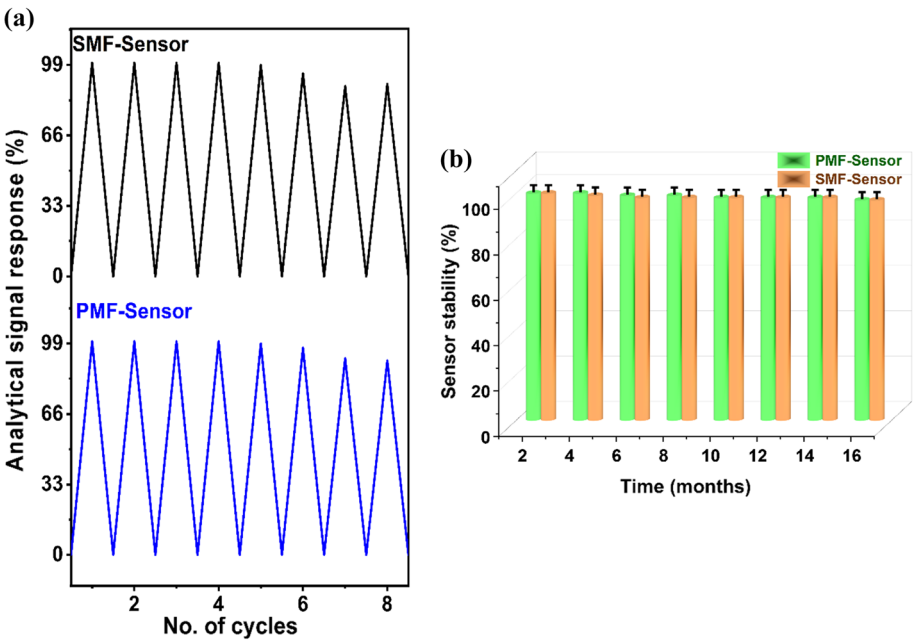

Figure 9 **a** Reusability assay and **b** stability analysis of the proposed PMF and SMF sensors.

reusability features make them the pressing analytical method for sensing diverse analytes of interest, which are otherwise impossible given the budget-to-demand ratio.

Acknowledgements

This work was supported by VIT (Seed Grant 2021-22) and IGCAR-Kalpakkam (IGCAR/M&MFCG/FChD/SCSS/01/2018/W.O.No.VITV-01).

Authors contributions

Akhila Maheswari M and Prabhakaran D were responsible for conceptualization, methodology, visualization, investigation, writing—reviewing and editing, funding acquisition, resources, supervision and project administration. Aswanidevi K was involved in formal analysis, methodology, data curation, investigation, validation, writing and preparing the original draft and software.

Declarations

Conflict of interest The authors declare that there is no conflict of interest concerning the publication of this research work.

Supplementary Information: The online version contains supplementary material available at https://doi.org/10.1007/s10853-022-07765-w.

References

[1] Bismuth M, Zaltzer E, Muthukumar D et al (2021) Real-time detection of copper contaminants in environmental water using porous silicon Fabry–Pérot interferometers. Analyst 146:5160–5168. https://doi.org/10.1039/d1an00701g

[2] Pohl A (2020) Removal of heavy metal ions from water and wastewaters by sulfur-containing precipitation agents. Water Air Soil Pollut 231:503–520. https://doi.org/10.1007/s11270-020-04863-w

[3] Shamim MA, Zia H, Zeeshan M et al (2022) Metal organic frameworks (MOFs) as a cutting-edge tool for the selective detection and rapid removal of heavy metal ions from water: recent progress. J Environ Chem Eng 10:106991. https://doi.org/10.1016/j.jece.2021.106991

[4] Sivakumar M, Widakdo J, Hung W-S et al (2022) Porous graphene nanoplatelets encompassed with nitrogen and sulfur group for heavy metal ions removal of adsorption and desorption from single or mixed aqueous solution. Sep Purif Technol 288:120485. https://doi.org/10.1016/j.seppur.2022.120485

[5] Pengpumkiat S, Wu Y, Boonloed A et al (2017) A microfluidic detection system for quantitation of copper incorporating a wavelength-ratiometric fluorescent quantum

dot pair. Anal Methods 9:1125–1132. https://doi.org/10.1039/c6ay02718k

[6] da Silva DA, De Luca A, Squitti R et al (2022) Copper in tumors and the use of copper-based compounds in cancer treatment. J Inorg Biochem 226:111634. https://doi.org/10.1016/j.jinorgbio.2021.111634

[7] Zhang Z, Zhao W, Hu C et al (2022) Colorimetric copper (II) ions detection in aqueous solution based on the system of 3'3'5'5'-tetramethylbenzidine and AgNPs in the presence of $Na_2S_2O_3$. J Sci Adv Mater Devices 7:100420. https://doi.org/10.1016/j.jsamd.2022.100420

[8] Krishna Kumar S, Mohan AM (2021) Porous inorganic/organic hybrid monolith-based solid sensor for the colorimetric analysis of Cu^{2+} ions. J Nanoparticle Res 23:1–17. https://doi.org/10.1007/s11051-021-05316-z

[9] Isaad J, El AA (2022) Sequential colorimetric sensor for copper (II) and cyanide ions via the complexation−decomplexation mechanism based on sugar pyrazolidine-3,5-dione. J Mol Struct 1252:132151. https://doi.org/10.1016/j.molstruc.2021.132151

[10] Liu HT, Jiang SJ (2003) Determination of copper in coal fly ash in the presence of excess titanium by dynamic reaction cell inductively coupled plasma mass spectrometry. Anal Bioanal Chem 375:306–309. https://doi.org/10.1007/s00216-002-1681-4

[11] Afzali D, Mostafavi A, Taher MA, Moradian A (2007) Flame atomic absorption spectrometry determination of trace amounts of copper after separation and preconcentration onto TDMBAC-treated analcime pyrocatechol-immobilized. Talanta 71:971–975. https://doi.org/10.1016/j.talanta.2006.05.012

[12] Wang Z, Cai W, Hong W et al (2019) Multi-objective optimization design and performance evaluation of a novel multi-stream intermediate fluid vaporizer with cold energy recovery. Energy Convers Manag 195:32–42. https://doi.org/10.1016/j.enconman.2019.04.066

[13] Liu ZC, Qi JW, Hu C et al (2015) Cu nanoclusters-based ratiometric fluorescence probe for ratiometric and visualization detection of copper ions. Anal Chim Acta 895:95–103. https://doi.org/10.1016/j.aca.2015.09.002

[14] Gong H, Cheng Y, Zhang Y et al (2021) A novel fluorous effect induced fluorescence sensor for Cu(II) detection in the organic phase with high sensitivity. Mater Chem Front 5:5361–5370. https://doi.org/10.1039/d1qm00307k

[15] Bagheri N, Mazzaracchio V, Cinti S et al (2021) Electroanalytical sensor based on gold-nanoparticle-decorated paper for sensitive detection of copper ions in sweat and serum. Anal Chem 93:5225–5233. https://doi.org/10.1021/acs.analchem.0c05469

[16] Liang S, Tong Q, Qin X et al (2020) A hydrophilic naphthalimide-based fluorescence chemosensor for Cu^{2+} ion: sensing properties, cell imaging and molecular logic behavior. Spectrochim Acta–Part A Mol Biomol Spectrosc 230:118029. https://doi.org/10.1016/j.saa.2020.118029

[17] Wang H, Zhao S, Xu Y et al (2020) A new fluorescent probe based on imidazole[2,1-b]benzothiazole for sensitive and selective detection of Cu^{2+}. J Mol Struct 1203:127384. https://doi.org/10.1016/j.molstruc.2019.127384

[18] Vareda JP, Valente AJM, Durães L (2021) Ligands as copper and nickel ionophores: applications and implications on wastewater treatment. Adv Colloid Interface Sci 289:102364. https://doi.org/10.1016/j.cis.2021.102364

[19] Deepa A, Srinivasadesikan V, Lee SL, Padmini V (2020) Highly selective and sensitive colorimetric and fluorimetric sensor for Cu^{2+}. J Fluoresc 30:3–10. https://doi.org/10.1007/s10895-019-02450-9

[20] Mahnashi MH, Mahmoud AM, Alkahtani SA et al (2020) A novel imidazole derived colorimetric and fluorometric chemosensor for bifunctional detection of copper (II) and sulphide ions in environmental water samples. Spectrochim Acta–Part A Mol Biomol Spectrosc 228:117846. https://doi.org/10.1016/j.saa.2019.117846

[21] Liu Y, Wang L, Guo C, Hou Y (2018) A colorimetric squaraine-based probe and test paper for rapid naked eyes detection of copper ion (II). Tetrahedron Lett 59:3930–3933. https://doi.org/10.1016/j.tetlet.2018.09.042

[22] Mohammed GI, El-Ghamry HA, Saber AL (2021) Rapid, sensitive, and selective copper (II) determination using sensitive chromogenic azo dye based on sulfonamide. Spectrochim Acta–Part A Mol Biomol Spectrosc 247:119103. https://doi.org/10.1016/j.saa.2020.119103

[23] Golbedaghi R, Justino LLG, Ooshall F et al (2021) A new Schiff base ligand as a fluorescence probe for Cu(II) detection in semi-aqueous solution: synthesis, characterization, fluorescence and mechanistic insight. Inorganica Chim Acta 528:120623. https://doi.org/10.1016/j.ica.2021.120623

[24] Wu SP, Du KJ, Sung YM (2010) Colorimetric sensing of Cu(II): Cu(II) induced deprotonation of an amide responsible for color changes. Dalt Trans 39:4363–4368. https://doi.org/10.1039/b925898a

[25] Wang X, Liu G, Qi Y et al (2019) Embedded Au Nanoparticles-Based Ratiometric Electrochemical Sensing Strategy for Sensitive and Reliable Detection of Copper Ions. Anal Chem 91:12006–12013. https://doi.org/10.1021/acs.analchem.9b02945

[26] Wang S, Yu G, Ma Y et al (2019) Ratiometric Photoacoustic Nanoprobe for Bioimaging of Cu^{2+}. ACS Appl Mater Interfaces 11:1917–1923. https://doi.org/10.1021/acsami.8b20113

[27] Wu M, Suo F, Zhou J et al (2018) Paper-based fluorogenic device for detection of copper ions in a biological system. ACS Appl Bio Mater 1:1523–1529. https://doi.org/10.1021/acsabm.8b00435

[28] Deng X, Feng Y, Li H et al (2018) N-doped carbon quantum dots as fluorescent probes for highly selective and sensitive detection of Fe^{3+} ions. Particuology 41:94–100. https://doi.org/10.1016/j.partic.2017.12.009

[29] Satheeshkumar E, Yang J, Srinivasadesikan V, Lin MC (2017) Simultaneous production and surface functionalization of silver nanoparticles for label-free colorimetric detection of copper ion. Anal Sci 33:1115–1121. https://doi.org/10.2116/analsci.33.1115

[30] Awual MR, Hasan MM (2015) Colorimetric detection and removal of copper(II) ions from wastewater samples using tailor-made composite adsorbent. Sens Actuators, B Chem 206:692–700. https://doi.org/10.1016/j.snb.2014.09.086

[31] Awual MR, Hasan MM, Rahman MM, Asiri AM (2019) Novel composite material for selective copper(II) detection and removal from aqueous media. J Mol Liq 283:772–780. https://doi.org/10.1016/j.molliq.2019.03.141

[32] Sompalli NK, Deivasigamani P (2020) Structurally designed porous polymer monoliths as probe-anchoring templates as benign and fast responsive solid-state optical sensors for the sensing and recovery of copper ions. Nanotechnology 31:414004. https://doi.org/10.1088/1361-6528/ab9e2a

[33] Kongasseri A, Sompalli NK, C.V.S. Rao B, et al (2020) Solid-state optical sensing of ultra-trace Hg^{2+} ions using chromoionophoric probe anchored silica monolithic architectures. Sens Actuators, B Chem 321:128558. https://doi.org/10.1016/j.snb.2020.128558

[34] Sompalli NK, Mohan AM, Rao CVSB et al (2019) Tailor-made porous polymer and silica monolithic designs as probe anchoring templates for the solid-state naked eye sensing and preconcentration of hexavalent chromium. Sens Actuators, B Chem 298:126896. https://doi.org/10.1016/j.snb.2019.126896

[35] Kongasseri A, Deivasigamani P, Mohan AM (2022) Probe tethered monolithic architectures as facile solid-state chemosensors for the on-site colorimetric recognition of Co(II) in aqueous and industrial samples. Environ Res 203:111861. https://doi.org/10.1016/j.envres.2021.111861

[36] Sompalli NK, Kuppusamy S, Mohan AM et al (2022) Probe decorated porous silica and polymer monoliths as solid-state optical sensors and preconcentrators for the selective and fast recognition of ultra-trace arsenic ions. J Hazard Mater 421:126828. https://doi.org/10.1016/j.jhazmat.2021.126828

[37] Guli M, Yao J, Chen L et al (2014) Synthesis and characterization of mesoporous composite silica monolith. Adv Powder Technol 25:1262–1265. https://doi.org/10.1016/j.apt.2014.03.004

[38] Vlakh EG, Sergeeva YN, Evseeva TG et al (2011) Monodisperse polystyrene microspheres used as porogenes in the synthesis of polymer monoliths. Polym Sci–Ser A 53:172–182. https://doi.org/10.1134/S0965545X11020106

[39] Zhou Y, Gu FN, Gao L et al (2011) 3D net-linked mesoporous silica monolith: new environmental adsorbent and catalyst. Catal Today 166:39–46. https://doi.org/10.1016/j.cattod.2010.04.052

[40] Zheng H, Liu Q, Jia Q (2014) Preparation of poly(butyl methacrylate-co-ethyleneglyceldimethacrylate) monolithic column modified with β-cyclodextrin and nano-cuprous oxide and its application in polymer monolithic microextraction of polychlorinated biphenyls. J Chromatogr A 1343:47–54. https://doi.org/10.1016/j.chroma.2014.03.067

[41] Madhesan T, Mohan AM (2020) Porous silica and polymer monolith architectures as solid-state optical chemosensors for Hg^{2+} ions. Anal Bioanal Chem 412:7357–7370. https://doi.org/10.1007/s00216-020-02870-8

[42] Khalil MMH, Shahat A, Radwan A, El-Shahat MF (2016) Colorimetric determination of Cu(II) ions in biological samples using metal-organic framework as scaffold. Sensors Actuators, B Chem 233:272–280. https://doi.org/10.1016/j.snb.2016.04.079

[43] Sompalli NK, Deivasigamani P (2021) Fabrication of target specific solid-state optical sensors using chromoionophoric probe–integrated porous monolithic polymer and silica templates for cobalt ions. Anal Bioanal Chem 413:3177–3191. https://doi.org/10.1007/s00216-021-03255-1

[44] Liu T, Li G, Zhang N, Chen Y (2012) An inorganic-organic hybrid optical sensor for heavy metal ion detection based on immobilizing 4-(2-pyridylazo)-resorcinol on functionalized HMS. J Hazard Mater 201–202:155–161. https://doi.org/10.1016/j.jhazmat.2011.11.060

[45] Kuppusamy S, Deivasigamani P (2022) Porous carbon-based polymer monolithic template implanted with an ion-receptor molecular probe as a solid-state ocular sensor for the selective targeting and capturing of cobalt ions. New J Chem 46:398–406. https://doi.org/10.1039/d1nj04793k

[46] El-Safty SA, Prabhakaran D, Ismail AA et al (2007) Nanosensor design packages: a smart and compact development for metal ions sensing responses. Adv Funct Mater 17:3731–3745. https://doi.org/10.1002/adfm.200700447

[47] Kavitha S, Mary Jelastin Kala S, Anand Babu Christus A, Ravikumar A (2021) Colorimetric determination of cysteine and copper based on the peroxidase-like activity of Prussian blue nanocubes. RSC Adv 11:37162–37170. https://doi.org/10.1039/d1ra06838e

[48] Xie YQ, Zhang YM, Li ZH et al (2021) A novel highly sensitive dual-channel chemical sensor for sequential recognition of Cu^{2+} and CN^{-} in aqueous media and its bioimaging applications in living cells. New J Chem 45:18421–18432. https://doi.org/10.1039/d1nj03548g

[49] Yuan Z, Cai N, Du Y et al (2014) Sensitive and selective detection of copper ions with highly stable polyethyleneimine-protected silver nanoclusters. Anal Chem 86:419–426. https://doi.org/10.1021/ac402158j

[50] Sadollahkhani A, Hatamie A, Nur O et al (2014) Colorimetric Disposable paper coated with ZnO@ZnS core−shell nanoparticles for detection of copper ions in aqueous solutions. ACS Appl Mater Interfaces 6:17694–17701. https://doi.org/10.1021/am505480y

[51] Yan W, Zhong Z, Ma J, Rujiralai T (2021) Highly sensitive colorimetric sensing of copper(II) ions based on "CLICK-17" DNAzyme-catalyzed azide modified gold nanoparticles and alkyne capped dsDNA cycloaddition. RSC Adv 11:24196–24205. https://doi.org/10.1039/d1ra03813c

[52] Awual MR (2017) New type mesoporous conjugate material for selective optical copper(II) ions monitoring & removal from polluted waters. Chem Eng J 307:85–94. https://doi.org/10.1016/j.cej.2016.07.110

[53] Isaad J, El AA (2021) A novel sugar pyrazolin-5-one based optical chemosensor for sequential detection of copper (II) and cyanide ions in real samples. Experimental and theoretical studies. J Mol Struct 1228:129771. https://doi.org/10.1016/j.molstruc.2020.129771